Scaling analysis and application: Phase diagram of magnetic nanorings and elliptical nanoparticles

Wen Zhang,* Rohit Singh, Noah Bray-Ali, and Stephan Haas
Department of Physics and Astronomy, University of Southern California, Los Angeles, California 90089, USA
(Received 28 September 2007; revised manuscript received 3 April 2008; published 28 April 2008)

The magnetic properties of single-domain nanoparticles with different geometric shapes, crystalline anisotropies, and lattice structures are investigated. A recently proposed scaling approach is shown to be universal and in agreement with dimensional analysis coupled with the assumption of *incomplete* self-similarity. It is used to obtain phase diagrams of magnetic nanoparticles featuring three competing configurations: in-plane ferromagnetism, out-of-plane ferromagnetism, and vortex formation. The influence of the vortex core on the scaling behavior and phase diagram is analyzed. Three-dimensional phase diagrams are obtained for cylindrical nanorings depending on their height and outer and inner radii. The triple points in these phase diagrams are shown to be in a linear relationship with the inner radius of the ring. Elliptically shaped magnetic nanoparticles are also studied. A new parametrization for double vortex configurations is proposed, and regions in the phase diagram where the double vortex is a stable ground state are identified.

DOI: 10.1103/PhysRevB.77.144428 PACS number(s): 75.75.+a, 36.40.Cg, 61.82.Rx

I. INTRODUCTION

Magnetic thin films and nanoparticles have been intensively studied during the past two decades[1,2] not only because of their great potential for technological applications but also because of fundamental scientific interest. Many new phenomena come about by imposing geometric restrictions in one[1] or more dimensions.[3–6] It has been demonstrated that nanoparticles predominantly show a single-domain structure when their size is smaller than a characteristic length scale.[7] These single domain particles are promising candidates for high density data storage,[8] integrated magnetic-electronic devices,[9] and applications in biotechnology.[10]

A great deal of attention has focused on arrays of magnetic nanoparticles. In magnetic nanoparticle arrays, there are two distinct issues of interest: the spin configuration of the individual particles and the interactions between them. Here, we focus on the first issue. The magnetic properties obtained under this consideration are valid when the distance between the individual particles is larger than twice the characteristic size of the individual particles since it has been shown that the interactions can be safely neglected under this condition.[6,11]

Within nanoparticles, different magnetic configurations have been observed, including vortex, leaf, and flower states.[12] Single-domain configurations have attracted continuous attention for their obvious application potential. In particular, the magnetic vortex, which is also known as a nonlocalized soliton, has been recently explored for its application potential and interesting dynamics.[13–15] In this work, we study the magnetic phase diagrams of such nanostructures as a function of their shape, crystalline anisotropy, and lattice structure.

On the numerical side, a scaling approach has been shown to be effective in determining phase diagrams for cylinder[16] and cone[17] shaped nanoparticles. Here, we provide a systematic numerical study for different geometric shapes. When the characteristic length scale is sufficiently small, the shape of the particle is one of the dominant factors determining its magnetic properties. Numerous experimental investigations have addressed this and related issues of domain structure.[5,18]

On the conceptual side, the scaling approach suggests a self-similarity of magnetic nanoparticles.[19] Reference 20 tacitly assumes that magnetic nanoparticles exhibit complete self-similarity with respect to the small parameter a/L_{ex}, where a is the lattice spacing and L_{ex} is the magnetic exchange length. In fact, the particles exhibit only *incomplete* self-similarity with respect to the lattice spacing in certain circumstances, as we will demonstrate in this work. This incomplete similarity agrees with dimensional analysis, as it must, and with available numerical data.[16,17,21]

The topology of the nanoparticle plays an important role.[22–25] In a simply connected topology, vortex states, for example, typically must have a core region in which the spins point out of the vortex plane. In a nanoring, furthermore, the inner radius R_i provides an additional length scale with which to probe the self-similarity of magnetic nanoparticles. We perform a scaling analysis and show that nanoparticles in this topology exhibit *complete* similarity with respect to the lattice constant. This is a consequence of the additional length R_i that plays the role of the lattice constant in regulating the vortex core energy.

Quite a different scenario of the magnetization reversal was revealed in elliptical particles.[26–29] Numerical simulations showed different spin configurations including multivortex states.[30] The double vortex configuration confined in an elliptically shaped ferromagnetic particle is especially interesting because it provides a model system for studying static and dynamic interactions between solitons (localized solution of nonlinear equations).[26] Many efforts[30,31] have been taken to obtain the phase diagram of such systems; yet, it is still an open problem.

The first topic of this paper is to reveal the essence of the scaling approach and to verify its validity in terms of different shapes, anisotropies, and crystalline structures. Also, the effects of these parameters on the phase diagrams are analyzed. The influence of the vortex core on the scaling behavior and phase diagram is investigated. Furthermore, the scaling approach is applied to nanorings and elliptically shaped

nanoparticles. The resulting phase diagrams are given, and new and interesting phenomena are discussed.

II. MODEL AND NUMERICAL PROCEDURE

In the absence of an external magnetic field, the Hamiltonian ($\mathcal{H}$) (or energy) of a magnetic nanoparticle consists of three terms: exchange interaction, dipolar interaction, and crystalline anisotropy. If each magnetic moment occupies a site of the underlying lattice, $\mathcal{H}$ is given by

$$\mathcal{H} = -J\sum_{\langle i,j\rangle} \vec{S}_i \cdot \vec{S}_j + D\sum_{i,j} \frac{\vec{S}_i \cdot \vec{S}_j - 3(\vec{S}_i \cdot \hat{r}_{ij})(\vec{S}_j \cdot \hat{r}_{ij})}{r_{ij}^3} + U_k, \tag{1}$$

where $J>0$ is the ferromagnetic exchange constant (or exchange integral, which is measured in units of energy),[32] which is assumed to be nonzero only for nearest neighbors, D is the dipolar coupling parameter, and $\vec{r}_{ij}$ is the displacement vector between sites i and j. The anisotropy term U_k can take various forms,[32] among which the most common are uniaxial anisotropy, $U_k = K\Sigma_i \sin^2 \theta_i$, where θ_i is the angle $\vec{S}_i$ makes with the easy axis, and cubic anisotropy, $U_k = K\Sigma_i[\alpha_i^2\beta_i^2 + \beta_i^2\gamma_i^2 + \alpha_i^2\gamma_i^2]$, where $\alpha_i, \beta_i, \gamma_i$ are the direction cosines of $\vec{S}_i$. Note that K is the single site anisotropy energy (not an energy density). For most materials, the dimensionless ratio D/Ja^3 falls in the range of $10^{-3}-10^{-4}$, where the lattice constant a is approximately 3 Å. The dimensionless ratio Ka^3/D lies between 0 and 10. We choose $Ka^3/D=1$, $Ja^3/D=5000$, and $a=3$ Å in the following calculations unless they are specified otherwise.

The objects studied in this paper are magnetic nanoparticles with various shapes and anisotropies. In such systems, three dominant competing configurations have been identified:[16] (I) out-of-plane ferromagnetism with the magnetization aligned parallel to the nanodot base, (II) in-plane ferromagnetism with the magnetization perpendicular to the base, and (III) a vortex state with the magnetic moments circling in the base plane. Double vortex states in elliptically shaped particles will be discussed in detail later. A typical phase diagram for a cylinder is shown in Fig. 1, which exhibits these three phases as a function of the cylinder radius R and its height H. Note that there can be other metastable configurations, such as the buckle state,[33,34] which are not considered here. These states result from the competition between the exchange and dipolar interactions. The exchange interaction tends to align spins in the same direction, whereas the dipolar interaction encourages spins to minimize their magnetostatic energy, resulting in the shape anisotropy. Thus, spins align in plane in a flat disk, while they point out of plane in an elongated cylinder. The vortex state is also a result of dipolar interactions since it nearly eliminates the demagnetization field.

In order to obtain phase diagrams such as the one shown in Fig. 1, one could resort to an analytical calculation based on a continuum model. However, this approach is limited to highly symmetric shapes and magnetization configurations. An alternative is to use numerical simulations. These can be

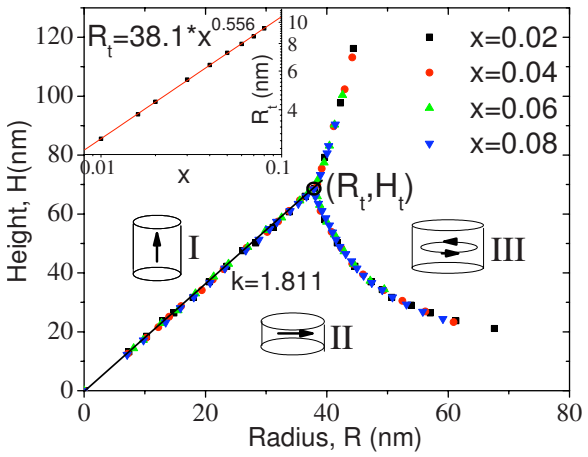

FIG. 1. (Color online) Scaled phase diagram of a cylindrical magnetic nanoparticle ($Ka^3/D=1$ and $Ja^3/D=5000$) as a function of its radius and height. The underlying lattice is simple cubic with $a=0.3$ Å. The three competing phases are (I) out-of-plane ferromagnetism, (II) in-plane ferromagnetism, and (III) the vortex state. The transition lines are obtained according to the scaling approach discussed in the text. The inset shows the dependence of the radius at the triple point on the scaling factor x.

powerful and universal but are often limited by the computational resource. As outlined in Ref. 16, the major technical problem is that the number of magnetic moments in systems of physical interest is of the order of 10^9, which cannot be presently handled even by high-end supercomputer facilities. To overcome this restriction, a scaling approach was recently proposed and demonstrated for cylinder[16] and cone[17] shaped nanoparticles. They showed that the phase diagram for an artificial small $J'=xJ$ $(x<1)$ could be scaled to the phase diagram for the original J according to $L'=x^{\eta}L$ ($\eta \simeq 0.55$ and L can be R,H). The phase boundary for small J' appears at small sizes, which involve less number of spins so that a lot of computing time is saved.

This proposal is equivalent to dimensional analysis coupled with a statement of incomplete similarity. We seek, for example, to find the height H separating the vortex phase from the ferromagnetic phase(s). In addition to the two governing parameters J,D explicitly appearing in Eq. (1), we also have the radius R of the cylinder and the lattice constant a. Thus, we seek a physical law for the critical height of the following form:

$$H = f(J,D,R,a). \tag{2}$$

From dimensional analysis, only two of the four governing parameters have independent dimensions. Following convention, we choose the independent parameters to be J and D, define the exchange length, $L_{ex}=a\sqrt{Ja^3/D}$, and express the scaling law in a dimensionless form:

$$\Pi = \Phi(\Pi_1, \Pi_2), \tag{3}$$

where $\Pi=H/L_{ex}$, $\Pi_1=R/L_{ex}$, $\Pi_2=a/L_{ex}$, and the scaling function Φ does not depend on the governing parameters of independent dimension, J,D.

Now, the typical values $a \sim 0.3$ nm, $L_{ex} \sim 20$ nm give $\Pi_2 \ll 1$. We are tempted to suggest complete similarity with respect to the small, dimensionless governing parameter Π_2.[19] Hence, we consider the limit $\Pi_2=0$:

$$\Pi = \Phi(\Pi_1,0) \equiv \Phi_1(\Pi_1), \tag{4}$$

where Φ_1 is independent of J, D, and a. By recasting in the original variables, we have that $H=L_{ex}\Phi_1(R/L_{ex})$. Notice now the invariance of this relation under the following rescaling of the governing parameters and critical height:

$$J' = xJ,$$

$$D' = D,$$

$$R' = x^{1/2}R,$$

$$a' = a,$$

$$H' = x^{1/2}H, \tag{5}$$

where x is any positive number. One way to see this is to notice that all lengths entering Eq. (4) get rescaled by the same amount $x^{1/2}$; thus, the dimensionless ratios Π, Π_1 are invariant. The invariance of Eq. (2) under this transformation is a consequence of dimensional analysis combined with complete similarity with respect to the dimensionless governing parameter $\Pi_2=a/L_{ex}$.

Interestingly, the numerical calculations under the assumption of a core-free vortex phase, where only the magnetic moment exactly located at the center of the vortex has a component pointing out of the vortex plane, do not obey this scaling.[16,17] Instead, they exhibit only incomplete similarity with respect to $\Pi_2=a/L_{ex}$.[19] Namely, for small values of $\Pi_2 \ll 1$, we have

$$\Pi = \Pi_2^{1-2\eta}\Phi_2\left(\frac{\Pi_1}{\Pi_2^{1-2\eta}}\right), \tag{6}$$

where the constant $\eta \approx 0.55$ does *not* follow from dimensional analysis. Here, Φ_2 is independent of J, D, and a. The special case of complete similarity is obtained when $\eta = 1/2$. This implies that the physical law Eq. (2) is *not* invariant under the transformation in Eq. (5). Rather, we find invariance under the modified transformation:

$$J' = xJ,$$

$$D' = D,$$

$$R' = x^{\eta}R,$$

$$a' = a,$$

$$H' = x^{\eta}H. \tag{7}$$

This is precisely the transformation described in Ref. 16 and is a consequence of dimensional analysis combined with incomplete similarity with respect to the small dimensionless parameter $\Pi_2=a/L_{ex}$. This incomplete similarity results from the fact that there is a singularity in the magnetization function.

Whenever we are presented with a scaling phenomenon such as Eq. (6), we have the opportunity to save considerable computational and experimental effort. The scaling law expresses a physical similarity between systems with different values of the governing parameters, so that we can use one to study the other. In particular, the authors of Ref. 16 suggested that we study small systems with a small exchange constant J, which are less computationally intensive to simulate. Then, we use Eq. (7) to scale up the results to the large systems with a large exchange constant that are of immediate physical and technological interest. The proposal is justified by the incomplete similarity of the physical law Eq. (2) with respect to the small, dimensionless parameter $\Pi_2=a/L_{ex}$. Other physical quantities of nanomagnets may satisfy incomplete similarity, including dynamic and thermal properties.[11,21,35]

III. RESULTS AND DISCUSSION

A. Shape, anisotropy, and lattice structure

Incomplete similarity with respect to the lattice constant occurs in magnetic nanoparticles regardless of cross-sectional geometry, crystalline anisotropy, or lattice structure. To illustrate the use of the scaling procedure, let us first consider the example of a cylindrical nanoparticle. By using the 2000-node, 15.78 teraflop high-performance supercomputer at the University of Southern California (USC), the energies of the competing phases were evaluated throughout the parameter plane spanned by the cylinder radius R and height H for systems with up to 400 000 sites. The scaling procedure was then used to collapse the resulting phase diagrams with different scaling factors, four of which ($x=0.02$, 0.04, 0.06, and 0.08) are given in Fig. 1 as examples. Note that there is a triple point (R_t,H_t), which is used to extract the scaling exponent, which is shown in the inset of Fig. 1. For the sake of simplicity, a simple cubic underlying lattice structure with cubic crystalline anisotropy and the "core-free" vortex state is adopted. Discussion about other structures and the effect of the core will come later.

The scaling exponent $\eta=0.556$ is consistent with the previous result,[16] suggesting incomplete similarity with respect to the lattice constant in this case. It is observed that the slope of the line separating the two ferromagnetic phases is $k=1.811$, which is in exact agreement with the analytical solution previously[36] given and argued.[20]

Since an enormously wide range of magnetic properties can be obtained by using different geometric shapes,[5] it is of great interest to see whether nanoparticles with different cross-sectional geometries exhibit incomplete similarity as well. To answer this question, here, we consider prism shaped nanoparticles with triangular, square, pentagonal, and hexagonal cross sections. From the results shown in Fig. 2(a), we find that within an error bar of 2%, these different geometries have the same scaling exponent showing incomplete similarity. In spite of the apparently universal scaling behavior, it is also evident that different geometries do favor different spin configurations. More precisely, the more sym-

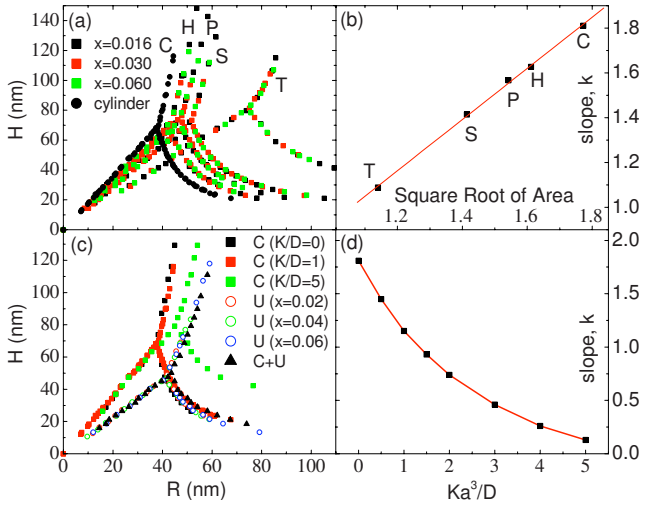

FIG. 2. (Color online) (a) Scaled phase diagrams for prism shaped nanoparticles. The radii R are defined as the distance from the base center to the corner of the polygons. The extracted scaling exponents for the triangle (T), the square (S), the pentagon (P), and the hexagon (H) are 0.556, 0.557, 0.563, and 0.559, respectively. (b) The slope (k) of the line separating phases I and II versus the square root of the cross-section area of the nanodot with unit radius. (c) Phase diagrams of cylindrical nanoparticles with different anisotropies. The solid squares represent the cubic anisotropy (C) of different magnitudes. The open circles with different colors represent the uniaxial anisotropy (U) with $Ka^3/D=1$ showing a valid scaling behavior with $\eta=0.56$. The solid triangles represent the combination of both anisotropies (U+C) with $Ka^3/D=1$. (d) The slope k versus the strength of the uniaxial anisotropy.

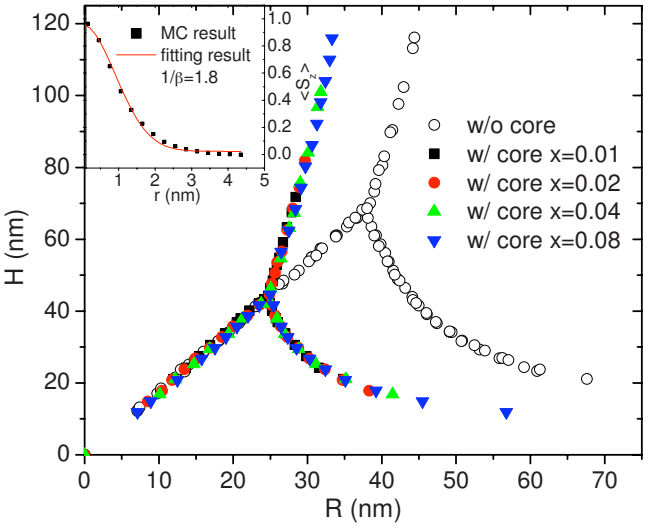

FIG. 3. (Color online) Scaled phase diagram of a single-domain cylindrical magnetic nanoparticle taking the vortex core into consideration. The black hollow circles represent the phase diagram for a cylindrical nanoparticle with the core-free model taken from Fig. 1. The scaling exponent $\eta=0.5$. The inset shows the fitting of the core function to the MC result for the case of $J'/D=100$.

metric the cross section is, the more the vortex phase is favored. Obviously, a cylindrical nanodot favors the vortex configuration the most. Another property of interest is the slope k of the line separating the two ferromagnetic (FM) phases. Figure 2(b) shows this slope as a function of the cross-section area. To compare the various polygon shapes, they have been normalized such that the distance from the corner of each polygon to its center is unity. The slope is found to increase with the basal area. This trend is easy to understand since the two FM configurations are determined by dipolar interactions, i.e., via the demagnetizing field, which, in turn, is related to the surface area. Quantitatively, the slope is expected to be approximately proportional to the square root of the area, which is found to be in agreement with the numerical results shown in Fig. 2(b).

In the following analysis of the universality of scaling for various crystalline anisotropies and underlying lattice structures, we will focus on cylindrical shapes for the simple reason that these are most commonly found in the existing experimental literature. Figure 2(c) gives the phase diagrams for the different anisotropies. In accordance with intuition, the cubic anisotropy equally favors the two ferromagnetic phases, i.e., the slope separating these two phases does not depend on Ka^3/D and at the same time suppresses vortex formation. Hence, one should consider materials with a *small* cubic anisotropy if one wishes to stabilize the vortex state. Besides the cubic anisotropy, another prevalent type is the uniaxial anisotropy. This anisotropy typically exists in hexagonal close-packed (hcp) lattices, but it can also occur in cubic lattices due to coupling to the substrate or other parts of the environment. In our calculation, the easy axis is set to be along the axis of the cylinder. The resulting phase diagram is shown in Fig. 2(c). We observe that the uniaxial anisotropy does not affect the scaling behavior and exponent. However, a feature worth mentioning is that the uniaxial anisotropy does change the slope of the line separating the two ferromagnetic phases, favoring the out-of-plane alignment (phase I). The larger the value of Ka^3/D is, the smaller the slope is [see Fig. 2(d)]. Meanwhile, when both anisotropies are present, the slope is dominated by the uniaxial term. Hence, an analysis of this slope can be used to experimentally determine the uniaxial anisotropy based on the information given in Fig. 2(d).

Various lattice structures exist in nature. It is important to know whether the scaling technique depends on the lattice structure. We calculated the phase diagram for hcp and face centered cubic lattices and their variance by rotating the lattice structure in the cylinder. The results remain invariant as long as all parameters (Ja^3/D, Ka^3/D, and density of spins) are kept the same and x is not too small. The above results indicate that the scaling behavior is robust to the details of the lattice structure, crystalline anisotropy, and geometric shape.

B. Particles with core structure

Interestingly, magnetic nanoparticles with a core structure exhibit complete similarity with respect to the lattice constant (see Fig. 3). Similar effects were reported by Landeros *et al.*[37] To analyze the effect of the core, we choose an ansatz $[S_z=\exp(-2r^2\beta^2)]$ introduced by Feldtkeller and Thomas.[38] We fit the results of Monte Carlo (MC) simulations with this

ansatz and obtain acceptable agreement (see the inset of Fig. 3). From dimensional analysis, the core size $1/\beta$ obeys a scaling law of the following form:

$$1/\beta = L_{\mathrm{ex}}\Phi_{\beta}(R/L_{\mathrm{ex}}, H/L_{\mathrm{ex}}, a/L_{\mathrm{ex}}), \tag{8}$$

where L_{ex} is the magnetic exchange length, as before, and Φ_{β} is a scaling function independent of J, D. Numerically, we find that the scaling function Φ_{β} is approximately independent of all its arguments, roughly giving $1/\beta \approx 0.6 L_{\mathrm{ex}}$. We use this as an additional governing parameter in the numerical calculations.

In the presence of the core, the critical height now satisfies a physical law of the following form:

$$H = g(J, D, R, a, 1/\beta). \tag{9}$$

From dimensional analysis, we find again only two independent governing parameters, define L_{ex}, and write

$$H = L_{\mathrm{ex}}\Phi_{g}[R/L_{\mathrm{ex}}, a/L_{\mathrm{ex}}, 1/(\beta L_{\mathrm{ex}})]. \tag{10}$$

Numerically, we find that Φ_g approaches a constant as its second argument a/L_{ex} becomes small. This is evidenced by the collapse of the phase diagrams in Fig. 3 with $\eta = 1/2$. The collapse implies invariance under the transformation in Eq. (5) and, thereby, the complete similarity with respect to the lattice constant. However, this is consistent with the incomplete similarity with respect to one exhibited in the core-free approach since we have an additional dimensional length $1/\beta$ that plays the role of the lattice constant. Similar results are obtained in Sec. III C when we change the topology of the nanoparticle and introduce an inner radius.

As to the phase diagram itself, the core significantly stabilizes the vortex configuration, pushing the phase boundary between FM and the vortex phase to smaller values of R and H by about 35%. Similar effects would affect Figs. 2(a) and 2(c) as well.

C. Cylindrical nanorings

Next, we consider the effects of changes in topology on the phase diagram. More precisely, we investigate the phase diagram of hollow cylinders, i.e., a nanoring structure characterized by an inner radius R_i, an outer radius R, and a height H. We find, as in Sec. III B, that the critical height exhibits complete similarity with respect to the lattice constant ($\eta \approx 1/2$). This is a consequence of the additional length R_i that plays the role of the lattice constant in regulating the vortex core energy.

Figure 4 shows three-dimensional phase diagrams in the (R_i, R, H) parameter manifold of the nanoring topology for two different values of the exchange couplings J'. Again, one observes two ferromagnetic regimes at small (R, H) values, competing with a vortex phase at larger (R, H). Moreover, one finds that for larger inner radii R_i, the vortex phase is more extended. This confirms the idea that the ring structure stabilizes the vortex configuration. The reason for this is that the core area, which typically pays a high energy penalty, is deliberately avoided in the ring structure. Another new feature of these phase diagrams is that the line separating the two ferromagnetic phases is not straight anymore.

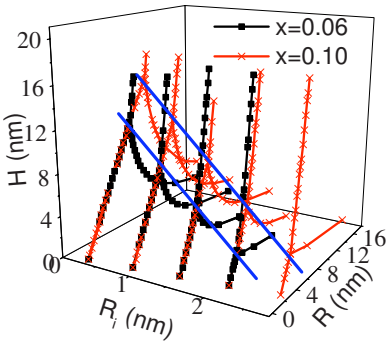

FIG. 4. (Color online) Phase diagrams of a cylindrical nanoring for two different x. There are two competing ferromagnetic phases at small (R, H) and a vortex phase at large (R, H). Because of the finite inner radius R_i, the onset of the phase transition line between the two ferromagnetic phases is shifted to finite values of R. Also, the vortex regime is more extended for larger R_i. The blue lines are guides to the eye, indicating that the triple points approximately form a straight line.

Instead, it now starts at finite $R = R_i$, and its slope smoothly changes to 1.81 as the ratio between R and R_i becomes very large. This relationship can be clearly observed in Fig. 5(a), which is derived from Eqs. (11) and (13) of Ref. 23. Here, we calculate the relationship between the critical height $H_c(R, R_i)$ as a function of $(R - R_i)$, resulting in the "star" symbols in Fig. 5(b), which exactly align with the line of our numerical calculation. Finally, the most surprising feature of the phase diagrams in Fig. 4 is that the triple points (R_t, H_t)

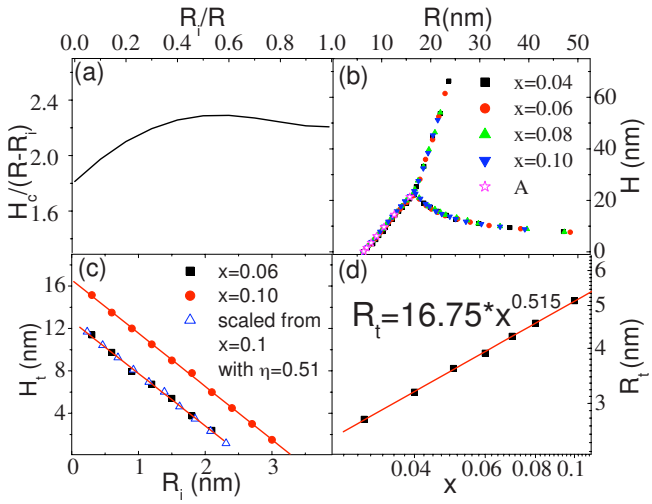

FIG. 5. (Color online) (a) For cylindrical nanorings, the phase transition line $H_c(R, R_i)$ separating the two ferromagnetic regimes is not straight, which is in contrast to the topologically connected objects discussed above. (b) Phase diagram for a cylindrical nanoring ($R_i = 6.3$ nm, $J/D = 5000$). The data "A" represent analytical phase transition lines calculated from (a), which are observed to coincide with the numerical results. (c) Height at the triple point (H_t) versus inner radius (R_i). The best fit for $x = 0.1$ is $H_t = 16.5 - 5(\pm 0.03) \times R_i$, whereas the best fit for $x = 0.06$ is $H_t = 12.7 - 4.95(\pm 0.09) \times R_i$. Hence, the two lines are approximately parallel and can thus be collapsed via scaling with $\eta = 0.51$. (d) The triple point radius (R_t) versus x.

for different R_i approximately form a straight line indicated by the two blue lines. This property is more clearly shown in Fig. 5(c), i.e., cylinder height at the triple point (H_t) versus R_i. It gives us a critical R_{ic} beyond which no in-plane ferromagnetic phase exists.

Another observation worth mentioning is that the intersect phase diagram in the $R_i=0$ plane of the cylindrical nanoring does not exactly coincide with the phase diagram of the simply connected cylinder (Fig. 1). It is closer to the case when the core structure is considered (Fig. 3). This phenomenon happens for the scaling exponent as well, which will be discussed right below.

One last feature to be discussed here is that the line connecting H_t [see Figs. 4 and 5(c)] is parallel for different values of the exchange coupling J'. By comparing the two phase diagrams for different J', we anticipate that a scaling behavior exists here as well as long as all three coordinates (R_i,R,H) are scaled. However, some difficulties arise since R_i should be different for different J', meaning that one would need to know the scaling exponent η in advance. Luckily, we can estimate the value of η from Fig. 5(c) as the two straight lines should scale if there is a scaling behavior. Thus, we first attempt to scale these two lines and find that they fit best when $\eta \simeq 0.51$. Then, we use this η to scale R_i and attempt to see whether the scaling behavior holds. Figure 5(d) shows the result. The scaling exponent is $\eta=0.515$, which is within 1% of the estimated value of 0.51. It is much closer to 0.5 in the finite core case, implying complete self-similarity since an additional length R_i is added and neglecting the core structure in the vortex state has little effect for a ring structure. With these results, we can easily calculate the critical inner radius $R_{ic} \simeq 11$ nm for the parameters we choose, above which a flat nanoring is always in the vortex phase. This is quite small compared to typical nanorings experimentally fabricated[22] and suggests that nanorings are generically in the vortex phase since they are typically flat with the height small compared to the width.

D. Elliptically shaped particles

It has been recently observed that a double vortex configuration exists in elliptically shaped ferromagnetic particles.[27,28,30,31] The full phase diagram for this case as a function of height, semimajor axis (R_a), and semiminor axis (R_b), however, has not yet been calculated. One of the difficulties in determining this phase diagram, using the technique outlined above, lies in finding an adequate parametrization of the double vortex state. The naive approximation of two single vortices is far from satisfying [see Fig. 6(c)]. As we will see below, the energy of two single vortices with discontinuous magnetization along the minor axis is significantly higher than that of a true double vortex with continuously varying magnetization [see Fig. 6(a)]. Without an accurate parametrization of the double vortex, one could only rely on Monte Carlo or micromagnetic simulations, which are extremely time consuming, and this would make it impossible to obtain a complete phase diagram.

Here, we propose a simple function to parametrize the double vortex. In our Monte Carlo simulations, we observe

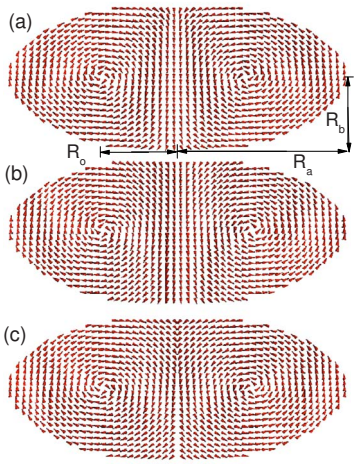

FIG. 6. (Color online) Double vortex configuration for $J/D=10$ ($x=0.002$), $R_a/R_b=2$ (the arrows represent the directions of magnetization). (a) Monte Carlo simulation result, $ea^3/D=21.12$. (b) Our parametrization, $ea^3/D=21.11$, $\mathcal{F}$ between b and a is 0.990. (c) Naive parametrization (two single vortices), $ea^3/D=20.91$, $\mathcal{F}$ between c and a is 0.974. e is the energy per spin and $\mathcal{F}$ is the fidelity defined in the text.

that the shape of the double vortex [Fig. 6(a)] looks much like the equipotential lines of two electric point charges with opposite signs placed at the centers of the vortex cores [Fig. 6(b)]. By symmetry, these cores should lie on the major axis of the ellipse. Let the distance from the core centers to the center of the ellipse be R_o. Then, the vector field $\vec{S}(\vec{r})$ is given by

$$\vec{S}(x,y) = \frac{-E_y\hat{i} + E_x\hat{j}}{E_x^2 + E_y^2}, \tag{11}$$

where

$$E_x = \frac{x - R_o}{[(x-R_o)^2 + y^2]^{3/2}} - \frac{x + R_o}{[(x+R_o)^2 + y^2]^{3/2}},$$

$$E_y = \frac{y}{[(x-R_o)^2 + y^2]^{3/2}} - \frac{y}{[(x+R_o)^2 + y^2]^{3/2}}.$$

Interestingly, the optimal positions of the vortex cores yielding the lowest energy configurations do not coincide with the ellipse foci but are located at nontrivial positions on the major axis with constant $\kappa=R_o/R_a$. κ almost exclusively depends on the aspect ratio R_a/R_b and only very weakly depends on size. Within the range we examined ($H<40$ nm, $R_a<30$ nm), κ decreases by only 2% as the size is increased. For different aspect ratios, we find $\kappa=0.44\pm0.1$. These values coincide with recent experimental results.[26–28] We choose $R_a/R_b=2$ as an example. In this case, $\kappa=0.44$. To quantify the quality of our parametrization of the double vortex, we look at the energy per spin (e) and the fidelity $\mathcal{F}=N^{-1}\Sigma_i \vec{S}_i \cdot \vec{S}'_i$, i.e., defined as the average dot product of spins on each lattice point of two configurations, $\vec{S}(\vec{r})$ and $\vec{S}'(\vec{r})$. The energy of our parametrization [Fig. 6(b)] is significantly closer to the energy obtained by Monte Carlo

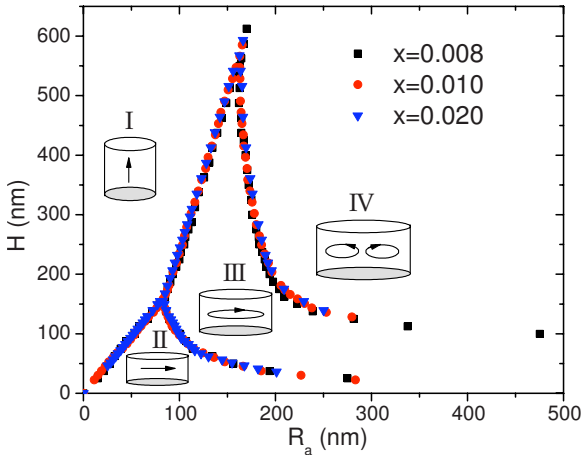

FIG. 7. (Color online) Scaled phase diagram of an elliptically shaped magnetic nanoparticle ($Ka^3/D=1$ and $Ja^3/D=5000$) as a function of its semimajor axis (R_a) and height (H) with an aspect ratio of 2. The four competing phases are (I) out-of-plane ferromagnetism, (II) in-plane ferromagnetism, (III) single vortex state, and (IV) double vortex state. The scaling exponent is $\eta=0.55$.

[Fig. 6(a)] and its fidelity is significantly closer to 1 than that of the two single vortex parametrization [Fig. 6(c)]. This is important because the energies of the single vortex and the double vortex configurations are very close. If one uses the naive parametrization, the double vortex could never be the ground state.

By using the parametrization of the double vortex in Eq. (11), we now apply the scaling procedure to obtain the phase diagram for elliptically shaped particles (see Fig. 7). Since there is no good description for the core of the double vortex yet, a core-free system is assumed for simplicity. We estimate that the boundary will shift to lower values of R_a and H by about 35% when taking the core into consideration.

As expected, the double vortex state becomes stable when both the semimajor axis and height of the nanoparticle are increased. In the vicinity of the phase boundary between the single vortex and the double vortex states, the energies for the two configurations are very close, and hence, there could be a large metastable region close to this phase boundary where both states could exist in nature. This is likely the reason why both these configurations have been observed in experiments on the same particle.[26] Regarding the scaling exponent, $\eta=0.55$ is again observed in this core-free consideration, implying incomplete self-similarity.

Here, we have only focused on the double vortex state. When the system size and the aspect ratio are sufficiently large, it is possible that multivortex states emerge. Besides such complex single-domain structures, cross-tie domain walls[39] could exist in these structures as well. It would be highly interesting to know under which condition these configurations could be stabilized.

IV. CONCLUSIONS

In conclusion, we have extended and analyzed the hypothesis of physical similarity put forward in Ref. 16. Regardless of shape, anisotropy, or crystal structure, we find numerical evidence for incomplete similarity ($\eta=0.55$) with respect to the lattice constant a when a core-free model is assumed. Introducing additional small length scales, such as the core size or an inner radius, restores the *complete* similarity ($\eta=0.5$) since the new small length regulates the vortex core.

A three-dimensional phase diagram for the cylindrical ring structure was obtained and a linear relationship between the height (H_t) at the triple point and the inner radius (R_i) was found, which offers a straightforward way of calculating the critical inner radius above which no in-plane ferromagnetic phase exists. A new parametrization for double vortex configurations was proposed. This configuration was found to be the ground state when both the radius and height of the elliptically shaped magnetic particle are large. Finally, a new phase diagram for elliptical nanoparticles including a double vortex phase was determined.

ACKNOWLEDGMENTS

We would like to thank Yaqi Tao, Denis Koltsov, Ilya Krivorotov, and Jose d'Albuquerque e Castro for useful discussions concerning this topic as well as closely related problems. The computing facility is generously provided by the USC high-performance supercomputing center. We also acknowledge financial support by the U.S. Department of Energy under Grant No. DE-FG02-05ER46240.

*zhangwen@usc.edu

[1] K. De'Bell, A. B. Maclsaac, and J. P. Whitehead, Rev. Mod. Phys. **72**, 225 (2000).
[2] J. I. Martin, J. Nogues, K. Liu, J. L. Vicent, and I. K. Schuller, J. Magn. Magn. Mater. **256**, 449 (2003).
[3] Y. Henry, K. Ounadjela, L. Piraux, S. Dubois, J. M. Gorge, and J. L. Duvail, Eur. Phys. J. B **20**, 35 (2001).
[4] J. D. Burton, R. F. Sabirianov, S. S. Jaswal, E. Y. Tsymbal, and O. N. Mryasov, Phys. Rev. Lett. **97**, 077204 (2006).
[5] R. P. Cowburn, D. K. Koltsov, A. O. Adeyeye, and M. E. Welland, Europhys. Lett. **48**, 221 (1999).
[6] C. A. Ross, M. Farhoud, M. Hwang, H. I. Smith, M. Redjdal, and F. B. Humphrey, J. Appl. Phys. **89**, 1310 (2001).
[7] J. W. F. Brown, J. Appl. Phys. **39**, 993 (1968).
[8] S. Y. Chou, Proc. IEEE **85**, 652 (1997).
[9] S. Parkin, J. Xin, C. Kaiser, A. Panchula, K. Roche, and M. Samant, Proc. IEEE **91**, 661 (2003).
[10] K. O'Grady, J. Phys. D **36**, 13 (2003).
[11] J. Mejía-López, D. Altbir, A. H. Romero, X. Batlle, I. V. Roshchin, C. Li, and I. K. Schuller, J. Appl. Phys. **100**, 104319 (2006).
[12] R. P. Cowburn and M. E. Welland, Phys. Rev. B **58**, 9217

(1998).
[13] S. B. Choe, Y. Acremann, A. Scholl, A. Bauer, A. Doran, J. Stöhr, and H. A. Padmore, Science **304**, 420 (2004).
[14] B. Van Waeyenberge *et al.*, Nature (London) **444**, 461 (2006).
[15] K. Yamada, S. Kasai, Y. Nakatani, K. Kobayashi, H. Kohno, A. Thiaville, and T. Ono, Nat. Mater. **6**, 270 (2007).
[16] J. d'Albuquerque e Castro, D. Altbir, J. C. Retamal, and P. Vargas, Phys. Rev. Lett. **88**, 237202 (2002).
[17] J. Escrig, P. Landeros, J. C. Retamal, D. Altbir, and J. d'Albuquerque e Castro, Appl. Phys. Lett. **82**, 3478 (2003).
[18] R. P. Cowburn, A. O. Adeyeye, and M. E. Welland, Phys. Rev. Lett. **81**, 5414 (1998).
[19] G. Barenblatt, *Scaling* (Cambridge University Press, Cambridge, 2003), pp. 286–294.
[20] K. Y. Guslienko and V. Novosad, Phys. Rev. Lett. **91**, 139701 (2003).
[21] P. Vargas, D. Altbir, and J. d'Albuquerque e Castro, Phys. Rev. B **73**, 092417 (2006).
[22] C. L. Chien, F. Q. Zhu, and J. Zhu, Phys. Today **60**(6), 40 (2007).
[23] M. Beleggia, J. W. Lau, M. A. Schofield, Y. Zhu, S. Tandon, and M. DeGraef, J. Magn. Magn. Mater. **301**, 131 (2006).
[24] P. Landeros, J. Escrig, D. Altbir, M. Bahiana, and J. d'Albuquerque e Castro, J. Appl. Phys. **100**, 044311 (2006).
[25] V. P. Kravchuk, D. D. Sheka, and Y. B. Gaididei, J. Magn. Magn. Mater. **310**, 116 (2007).
[26] K. S. Buchanan, P. E. Roy, and M. Grimsditch, Nat. Phys. **1**, 172 (2005).
[27] J. Johnson, M. Grimsditch, V. Metlushko, P. Vavassori, B. Ilic, P. Neuzil, and R. Kumar, Appl. Phys. Lett. **77**, 4410 (2000).
[28] P. Vavassori, N. Zaluzec, V. Metlushko, V. Novosad, B. Ilic, and M. Grimsditch, Phys. Rev. B **69**, 214404 (2004).
[29] R. P. Cowburn, D. K. Koltsov, A. O. Adeyeye, M. E. Welland, and D. M. Tricker, Phys. Rev. Lett. **83**, 1042 (1999).
[30] N. Usov, C.-R. Chang, and Z.-H. Wei, J. Appl. Phys. **89**, 7591 (2001).
[31] N. A. Usov, C. R. Chang, and Z. H. Wei, Phys. Rev. B **66**, 184431 (2002).
[32] C. Kittel, *Introduction to Solid State Physics*, 7th ed. (Wiley, New York, 1996), pp. 565–566.
[33] R. P. Cowburn and M. E. Welland, Appl. Phys. Lett. **72**, 2041 (1998).
[34] K. L. Metlov and Y. P. Lee, Appl. Phys. Lett. **92**, 112506 (2008).
[35] J. Mejia-Lopez, P. Soto, and D. Altbir, Phys. Rev. B **71**, 104422 (2005).
[36] A. Aharoni, J. Appl. Phys. **68**, 2892 (1990).
[37] P. Landeros, J. Escrig, D. Altbir, D. Laroze, J. d'Albuquerque e Castro, and P. Vargas, Phys. Rev. B **71**, 094435 (2005).
[38] E. Feldtkeller and H. Thomas, Phys. Kondens. Mater. **4**, 8 (1965).
[39] K. Kuepper, M. Buess, J. Raabe, C. Quitmann, and J. Fassbender, Phys. Rev. Lett. **99**, 167202 (2007).